Available online at www.sciencedirect.com
SCIENCE DIRECT®
Journal of Computational Physics 199 (2004) 66–86
JOURNAL OF COMPUTATIONAL PHYSICS
www.elsevier.com/locate/jcp

Spectral collocation schemes on the unit disc

Wilhelm Heinrichs

Universität Duisburg-Essen, Ingenieurmathematik (FB 10), Universitätsstrasse 3, D-45117 Essen, Germany

Received 4 November 2002; received in revised form 21 January 2004; accepted 2 February 2004
Available online 18 March 2004

Abstract

Two spectral collocation schemes on the unit disc are presented. The first one is based on the mapping of Gordon and Hall. Here the unit square is directly mapped onto the unit disc by means of an interpolation technique. Unlike other Poisson solvers on the unit disc no polar coordinates are involved. Hence the usual problems with the singularity of polar coordinates are avoided. This is also shown for more complex geometries. The second method is based on a diameter approach where the collocation nodes are no more clustering in the center. Numerical results are presented which demonstrate the high accuracy of our new spectral collocation schemes.

AMS: 65N35; 65P30; 77C05

Keywords: Collocation; Spectral; Unit disc; Complex geometry; Poisson problem; Gordon and hall; Diameter approach

1. Introduction

A new spectral collocation scheme for the Poisson problem on the unit disc is introduced. An efficient Poisson solver is required in many applications. For instance, in computational fluid dynamics a splitting of the Navier–Stokes equations leads to Poisson or "Pseudo-Poisson" problems for the pressure [11–13]. Most Poisson solvers are based on finite difference or finite element methods. Here we consider spectral collocation schemes.

Spectral methods [3,10,20] employ global polynomials for the discretization of elliptic boundary value problems. They give very accurate approximations for smooth solutions with relatively few degrees of freedom. For the collocation scheme it is essential to employ a collocation grid based on Gauss– or Gauss–Lobatto nodes. Hence these methods are well suited for rectangular domains but for more complex geometries the distribution of collocation nodes is not clear. Since by a stretching any smooth star-shaped domain can be simply mapped onto the unit disc we consider Poisson problems on this domain. In the previous spectral literature the Poisson equation is transformed into polar coordinates and then solved by means of a combined Chebyshev (or Legendre) and Fourier expansion. Here we refer to the existing papers

E-mail address: wheinric@ing-math.uni-essen.de (W. Heinrichs).

0021-9991/$ - see front matter
doi:10.1016/j.jcp.2004.02.001

in [1,4,5,16,18,19,21]. Unfortunately, this transform leads to a coordinate singularity along the axis at the center $r = 0$. Hence most Poisson solvers involve additional "pole conditions" to capture the behaviour of the solution as $r \to 0$. This has been discussed in detail by several authors [5,16,21]. An alternative is the use of Gauss–Radau collocation nodes which exclude the center $r = 0$. Hence the singularity at the center is avoided and no extra pole condition is required. The algebraic systems can be efficiently solved by a two-step eigenvalue technique. For a more detailed description we refer to the paper of Chen et al. [4]. Here we use a mapping technique introduced by Gordon and Hall [8,9] which maps a square into a quadrilateral domain with curved boundaries. In particular, we use this mapping for the unit disc where the curved boundaries are the arcs of the unit circle. Here we avoid the typical problems of polar coordinates where the terms $1/r$ and $1/r^2$ lead to large condition numbers for $r \to 0$. This effect is quite strong since the collocation nodes are dense near the center $r = 0$. We observed similar problems for the mapping of the square onto the triangle [14,15]. For our method we observe the well known high spectral accuracy. This is demonstrated by numerical results which are compared to the results of Chen et al. [4], Eisen et al. [5], Huang et al. [16] and Shen [21]. Only in cases where the solution is explicitly given in r (e.g., $u = r^4$) the treatment with polar coordinates yields better results. This is due to the fact that these schemes use expansions in r. For the other examples we obtain comparable or even better convergence. This is also confirmed for more complex geometries where a comparison with the method of Chen et al. [4] shows that we obtain a much higher accuracy.

In the second part of the paper we present a polar coordinate approach based on the diameter. Here the clustering of collocation nodes near the center is also avoided. Similar results were already obtained by Fornberg [6,7] and Torres/Coutsias [23]. Instead of the radius we employ the diameter $r \in [-1, 1]$ which leads to a new distribution of collocation nodes. Now the nodes are only dense near the boundary of the unit disc but not in the center. By choosing an odd number of radial nodes the center is not a collocation point and we do not need any pole conditions. In the angular direction θ we use for $\theta > \pi$ a shift of $\pi/2N$ so that an overlap of collocation nodes can be avoided. From numerical experiments we still observe the high spectral accuracy. Clearly, the condition number is strongly improved and the effect of rounding errors is reduced. The good performance of our approach is also shown for more complex geometries.

The paper is organized as follows. In the next section we introduce the Poisson problem and the mapping of Gordon and Hall for the unit disc. This is followed by the spectral discretization in Section 3. Numerical results and their discussion are presented in Section 4. In Section 5 we extend this technique to more complex domains. Finally in Section 6 an improved spectral scheme with polar coordinates is presented.

2. The poisson problem and mapping

We consider the Poisson problem

$$\Delta u = f \text{ in } D, \tag{1}$$

$$u = g \text{ on } \partial D \tag{2}$$

on the unit disc

$$D = \{(x, y) : \ x^2 + y^2 < 1\}.$$

Here f, g denote given functions defined on D and its boundary ∂D. In order to apply spectral collocation schemes one has to define a transformed problem on the square. Instead of introducing polar coordinates we prefer the mapping of Gordon and Hall [3,8,9]. They found a fairly simple interpolation procedure for mapping a square $Q = (-1, 1)^2$ into a quadrilateral with curved boundaries. We first use this mapping technique for mapping Q onto the disc

$$D^* = \sqrt{2}D = \{(x,y) : \ x^2 + y^2 < 2\}.$$

The boundary ∂D^* intersects with the four corners of Q. Let the four parts of ∂D^* be denoted by $\Gamma_i, i = 1,\ldots,4$ where

$$\Gamma_1 = \{(x,y) : \ y = \sqrt{2-x^2}, \ -1 < x < 1\},$$

$$\Gamma_2 = \{(x,y) : \ x = -\sqrt{2-y^2}, \ -1 < y < 1\},$$

$$\Gamma_3 = \{(x,y) : \ y = -\sqrt{2-x^2}, \ -1 < x < 1\},$$

$$\Gamma_4 = \{(x,y) : \ x = \sqrt{2-y^2}, \ -1 < y < 1\}.$$

The corresponding sides of the square Q are denoted by $\hat{\Gamma}_i, i = 1,\ldots,4$. One uses mappings π_i from $\hat{\Gamma}_i$ to Γ_i to construct the mapping Ψ from Q to D^*. Following Gordon and Hall [3,8,9], the mapping Ψ can be expressed in terms of the π_i as follows:

$$\begin{aligned}\Psi(\xi,\eta) = {} & \frac{1-\eta}{2}\pi_3(\xi) + \frac{1+\eta}{2}\pi_1(\xi) + \frac{1-\xi}{2}\left[\pi_2(\eta) - \frac{1+\eta}{2}\pi_2(1) - \frac{1-\eta}{2}\pi_2(-1)\right] \\ & + \frac{1+\xi}{2}\left[\pi_4(\eta) - \frac{1+\eta}{2}\pi_4(1) - \frac{1-\eta}{2}\pi_4(-1)\right].\end{aligned}$$

The functions $\pi_i, \ i = 1,\ldots,4$ are given by

$$\pi_1(\xi) = \begin{pmatrix} \xi \\ \sqrt{2-\xi^2} \end{pmatrix}, \quad \pi_3(\xi) = \begin{pmatrix} \xi \\ -\sqrt{2-\xi^2} \end{pmatrix}, \qquad -1 < \xi < 1,$$

$$\pi_2(\eta) = \begin{pmatrix} -\sqrt{2-\eta^2} \\ \eta \end{pmatrix}, \quad \pi_4(\eta) = \begin{pmatrix} \sqrt{2-\eta^2} \\ \eta \end{pmatrix}, \qquad -1 < \eta < 1.$$

By using these formulas the mapping can explicitly be written as

$$x = \xi\sqrt{2-\eta^2}, \quad y = \eta\sqrt{2-\xi^2}.$$

This defines the mapping of Q onto D^*. Finally one obtains D by the stretching

$$(x,y) \to (x,y)/\sqrt{2}.$$

Since we are interested in the solution of the Poisson problem we have to transform the Laplace operator into the coordinates of Q. The coordinates (x,y) of D are considered as a function of the coordinates (ξ,η) of Q, i.e., $x = x(\xi,\eta)$, $y = y(\xi,\eta)$. The partial derivatives are now transformed as follows:

$$\begin{bmatrix} x_\xi & y_\xi & 0 & 0 & 0 \\ x_\eta & y_\eta & 0 & 0 & 0 \\ x_{\xi\xi} & y_{\xi\xi} & x_\xi^2 & 2x_\xi y_\xi & y_\xi^2 \\ x_{\xi\eta} & y_{\xi\eta} & x_\xi x_\eta & x_\xi y_\eta + x_\eta y_\xi & y_\xi y_\eta \\ x_{\eta\eta} & y_{\eta\eta} & x_\eta^2 & 2x_\eta y_\eta & y_\eta^2 \end{bmatrix} \begin{bmatrix} u_x \\ u_y \\ u_{xx} \\ u_{xy} \\ u_{yy} \end{bmatrix} = \begin{bmatrix} u_\xi \\ u_\eta \\ u_{\xi\xi} \\ u_{\xi\eta} \\ u_{\eta\eta} \end{bmatrix}. \tag{3}$$

By inverting the above matrix and taking the sum of the third and fifth row we exactly obtain the coefficients of the transformed Laplace operator in (ξ, η) coordinates. Now we are able to apply spectral collocation schemes.

3. Spectral collocation

On Q we employ the standard Chebyshev Gauss–Lobatto collocation nodes given by

$$(\xi_i, \eta_j) = \left(\cos\frac{i\pi}{N}, \cos\frac{j\pi}{N} \right), \quad i, j = 0, \ldots, N.$$

By using the described mapping technique of Gordon and Hall we map these collocation nodes onto the disc D. For $N = 24$ they are plotted in Fig. 1. Clearly, they are clustering near the points $(x, y) = (\pm 1/\sqrt{2}, \pm 1/\sqrt{2})$ on which the four corners of Q are mapped. A zoom of the collocation nodes near $(x, y) = (1/\sqrt{2}, 1/\sqrt{2})$ is presented in Fig. 2. The partial derivatives of x, y and u in ξ and η are derived by means of the spectral collocation operators. In the following we write the spectral derivatives in matrix notation. First one has to introduce the transformation matrices from the space of function values to the space of (Chebyshev) coefficients. Since we employ a Chebyshev expansion we obtain the following matrix:

$$T = \cos\left(k\frac{i\pi}{N} \right), \quad i, k = 0, \ldots, N.$$

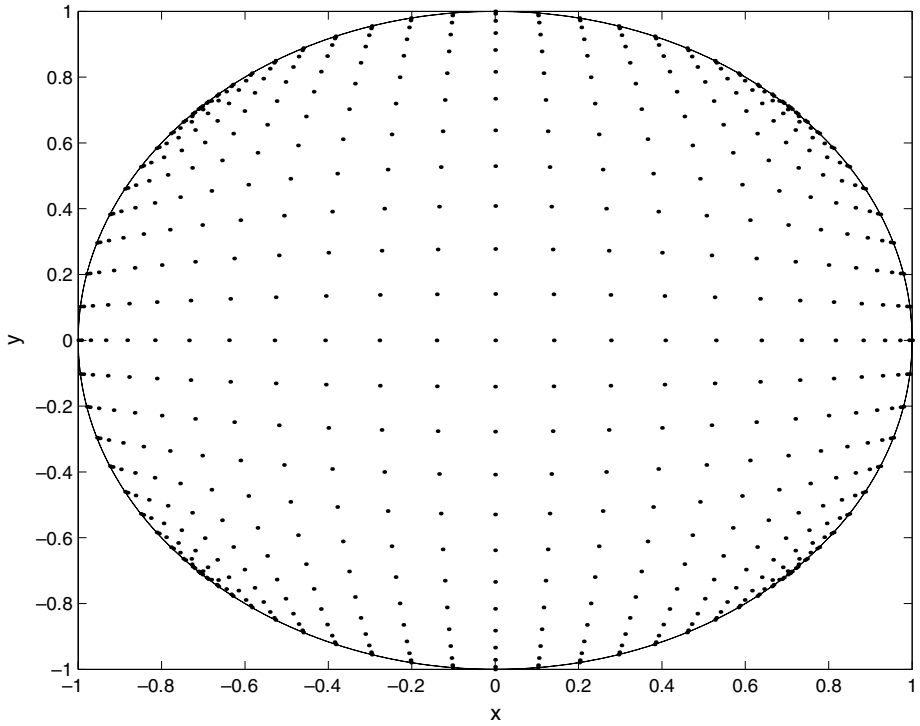

Fig. 1. Collocation nodes on the unit disc.

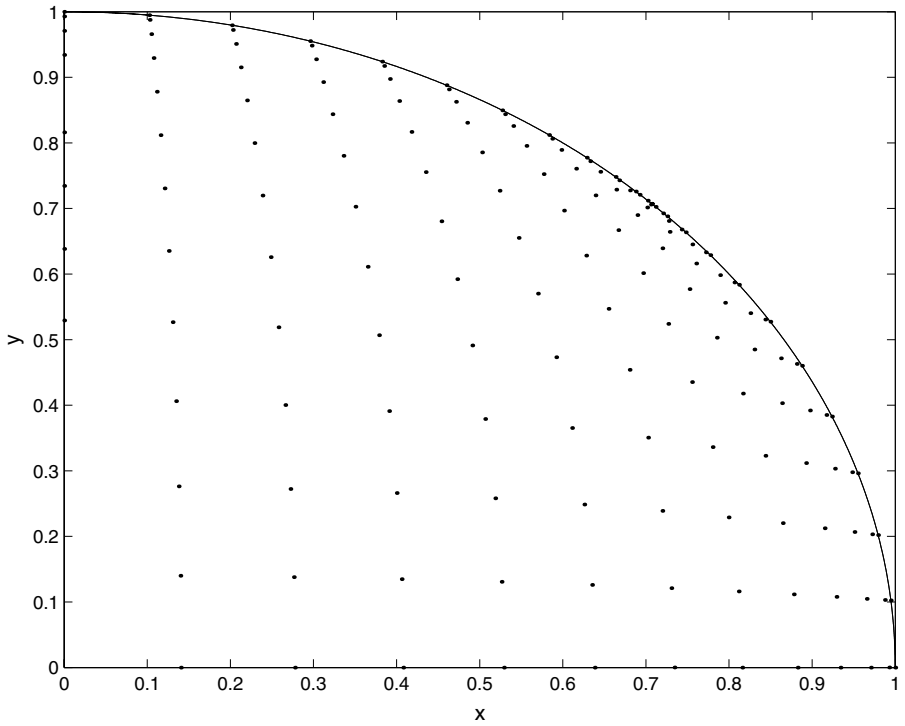

Fig. 2. Zoom of collocation nodes.

Further we need the differentiation matrix in the Chebyshev coefficient space which is explicitly given by $\hat{D} = (d_{i,j}) \in \mathbb{R}^{N+1,N+1}$ with

$$d_{i,j} = \begin{cases} \frac{2j}{c_i} & j = i+1,\ \ i+3,\ldots,N, \\ 0 & \text{else} \end{cases}$$

and

$$c_i = \begin{cases} 2 & i = 0, \\ 1 & \text{else.} \end{cases}$$

Now we are able to write the first and second spectral derivative matrices D1 and D2. They are explicitly given by

$$\mathrm{D1} = T\hat{D}T^{-1}, \quad \mathrm{D2} = T\hat{D}^2T^{-1}.$$

The spectral operators can be efficiently evaluated by fast Fourier transforms (FFTs) in $\mathrm{O}(N \log N)$ arithmetic operations. We further introduce the identity matrix $I \in \mathbb{R}^{N+1,N+1}$. By tensor product representation

$$A \otimes B = \left(Ab_{i,j}\right)_{i,j},$$

we are now able to write the spectral derivatives in 2D. The first order partial derivatives are given by

$$\frac{\partial}{\partial \xi} \cong \mathrm{D1} \otimes I, \quad \frac{\partial}{\partial \eta} \cong I \otimes \mathrm{D1}.$$

The second order derivatives are defined by

$$\frac{\partial^2}{\partial\xi\,\partial\xi} \cong \mathrm{D2} \otimes I, \quad \frac{\partial^2}{\partial\xi\,\partial\eta} \cong \mathrm{D1} \otimes \mathrm{D1}, \quad \frac{\partial^2}{\partial\eta\,\partial\eta} \cong I \otimes \mathrm{D2}.$$

The 2D spectral operators can be efficiently evaluated by FFTs in $\mathrm{O}(N^2 \log N)$ arithmetic operations. Now it is an easy task to implement the collocation scheme.

4. Numerical results

Due to the singularity of the above mapping (corners are mapped onto the smooth parts of the circle) a large condition number can be expected. In Table 1, we compared the condition numbers of the spectral Laplace operator evaluated on D respectively Q. They are numerically evaluated in the spectral norm and are denoted by

$$\mathrm{cond}_2^D, \ \mathrm{cond}_2^Q.$$

From the numerical results we observe that the condition number on D is about 2–3 orders of magnitude larger than on Q. For time-dependent problems this leads to prohibitively small time steps which is typical for such kind of singular mappings. Here we recommend implicit time schemes. However, we consider stationary problems and are interested in the spectral accuracy of the method. For this purpose we calculated the discrete L^∞ and L^2-errors on D. They are denoted by E_∞^D and E_2^D where

$$E_\infty^D = \max\{|\ (u - u_N)(x_i, y_j)\ |\colon\ i, j = 0, \ldots, N\}$$

and

$$E_2^D = \frac{1}{N}\sqrt{\sum_{i,j=0}^{N}(u - u_N)^2(x_i, y_j)}.$$

The errors are once more compared to the corresponding results on Q which are denoted by E_∞^Q, E_2^Q. We consider an example [4,5,16] with a smooth solution given by

$$u(x, y) = \cos(7y + 8x + 0.7). \tag{4}$$

Table 1
Condition numbers on D and Q

N	cond_2^D	cond_2^Q
4	1.16×10^1	8.16×10^0
8	1.07×10^3	8.92×10^1
12	2.32×10^4	4.25×10^2
16	2.19×10^5	1.32×10^3
20	1.27×10^6	3.19×10^3
24	5.38×10^6	6.59×10^3
28	1.83×10^7	1.22×10^4
32	5.30×10^7	2.07×10^4
48	1.31×10^9	1.05×10^5
64	1.30×10^{10}	3.22×10^5

From Table 2 we observe that the large condition number does not affect the high spectral accuracy. The results on Q are only slightly better than on D. For $N = 28$ the precision of our machine (about 10^{-14}) is already achieved. Hence the singularity of the mapping has nearly no influence on the accuracy. We further compared our method to the other schemes based on polar coordinates [4,5,16,21]. Here we have to notice that the cited references take

$$N_r = N, \quad N_\theta = 2N$$

for the polar coordinates (r, θ). Hence they employ $2N^2$ degrees of freedom whereas our method only requires N^2 degrees of freedom. Hence the computational costs are comparable if we here take $N = 12$. The error is measured in the L^∞-norm. We present numerical results (Table 3) for the above example and the additional examples

$$u(x, y) = e^{x+y}, \tag{5}$$

$$u(x, y) = \sqrt{x + y + 2}, \tag{6}$$

$$u(x, y) = \ln(x + y + 2), \tag{7}$$

$$u(x, y) = (x^2 + y^2)^2. \tag{8}$$

For the examples (4), (6) and (7) we obtain better results than the other references. For example (5) our results are similar to the others and for more complex geometries we also observe a good performance of our method (see Table 5). Only for example (8) we obtain much worse results. This is due to the fact that the exact solution $u = r^4$ can explicitly be written in r and hence the polar coordinate approaches yield exact results (up to machine precision). Clearly, for problems where the solution is an algebraic polynomial in r

Table 2
Numerical results for example (4)

N	E_2^D	E_∞^D	E_2^Q	E_∞^Q
4	5.12×10^{0}	1.49×10^{1}	6.76×10^{0}	1.79×10^{1}
8	8.73×10^{-2}	2.38×10^{-1}	7.02×10^{-2}	1.53×10^{-1}
12	1.73×10^{-3}	6.97×10^{-3}	8.76×10^{-4}	2.04×10^{-3}
16	7.81×10^{-6}	2.73×10^{-5}	3.44×10^{-6}	9.37×10^{-6}
20	1.44×10^{-8}	4.80×10^{-8}	5.44×10^{-9}	1.60×10^{-8}
24	1.60×10^{-11}	5.45×10^{-11}	4.12×10^{-12}	1.28×10^{-11}
28	2.35×10^{-13}	8.39×10^{-13}	1.28×10^{-14}	6.38×10^{-14}
32	2.10×10^{-13}	9.37×10^{-13}	2.00×10^{-14}	7.21×10^{-14}

Table 3
Numerical results for examples (4)–(8)

Example	Present	Chen [4]	Eisen [5]	Huang [16]	Shen [21]
$\cos(7x + 8y + 0.7)$	6.97×10^{-3}	3.96×10^{-1}	1.47×10^{0}	4.11×10^{-1}	–
e^{x+y}	3.87×10^{-7}	2.72×10^{-8}	3.27×10^{-6}	2.61×10^{-8}	2.6×10^{-8}
$\sqrt{x + y + 2}$	3.66×10^{-8}	1.80×10^{-5}	–	–	–
$\ln(x + y + 2)$	1.25×10^{-7}	1.34×10^{-4}	–	–	–
$r^4 = (x^2 + y^2)^2$	8.28×10^{-7}	8.63×10^{-15}	–	3.30×10^{-14}	–

or a trigonometric polynomial in θ the other approaches have better approximation properties. But in general our scheme is better or at least comparable to the methods with polar coordinates.

5. Complex geometry

Here we apply the mapping technique of Gordon and Hall to more complex geometries. We consider the Poisson problem on domains with smooth boundaries Γ which are parameterized in the arc length θ:

$$\Gamma(\theta) = \begin{pmatrix} d(\theta)\cos(\theta) \\ d(\theta)\sin(\theta) \end{pmatrix}, \quad 0 \leqslant \theta < 2\pi.$$

Here $d(\theta)$ denotes the radius in θ. The domain is normalized such that $d(\pi/4) = 1$. In order to apply the mapping technique of Gordon and Hall we have to define the mappings $\pi_i, i = 1, 2, 3, 4$. Here we only consider π_1. For given $\xi_j = \cos(j\pi/N), j = 0, \ldots, N$ one determines the arc length θ_j by solving the equation

$$d(\theta)\cos(\theta) = \xi_j$$

by a few steps (3–4 steps) of a Newton iteration. Then we obtain

$$\pi_1(\xi_j) = \begin{pmatrix} \xi_j \\ d(\theta_j)\sin(\theta_j) \end{pmatrix}. \tag{9}$$

A similar technique works for the other three mappings. Since the boundary curve is already given in a parameterized form it makes sense to define modified mappings $\hat{\pi}_i$ in the arc length θ. We once more describe this approach only for $\hat{\pi}_1$. First one maps the variable $\xi \in [-1, 1]$ onto $\theta \in [\pi/4, 3\pi/4]$ by

$$\theta = \theta(\xi) = \frac{\pi}{4}(2 - \xi).$$

Then for given ξ_j we determine $\theta_j = \theta(\xi_j)$ and obtain

$$\hat{\pi}_1(\xi_j) = \begin{pmatrix} d(\theta_j)\cos(\theta_j) \\ d(\theta_j)\sin(\theta_j) \end{pmatrix}. \tag{10}$$

A similar approach works on the other three parts of the boundary. By a numerical simulation we compared both approaches. We consider boundary curves given by

$$\hat{d}(\theta) = 1 + \sin^2(k\theta), \quad k = 0, 1, 2, \tag{11}$$

which are normalized such that $d(\pi/4) = 1$, i.e.,

$$d(\theta) = \hat{d}(\theta)/\hat{d}\left(\frac{\pi}{4}\right), \quad k = 0, 1, 2. \tag{12}$$

For $k = 0$ we reobtain the unit disc and for $k = 1, 2$ the boundaries become more complex. In Figs. 3 and 4 we plotted the distribution of collocation nodes for $k = 1, 2$ due to the parameterized mapping (10). We numerically calculated the discrete L^2-error for the Poisson problem with the exact solutions (4) and (5). The errors are denoted by E_2 for mapping (9) and E_2^{p} for the parameterized mapping (10). The corresponding results are presented in the Tables 4 and 5 for $k = 0, 1, 2$. On the unit disc ($k = 0$) mapping (9) yields the most accurate results. For more complex domains ($k = 1, 2$) the parameterized version (10) becomes better. This could be expected since a discretization along the arc length yields a higher order resolution of the boundary. Clearly, for increasing k the spectral accuracy is somewhat disturbed. For $k \geqslant 3$

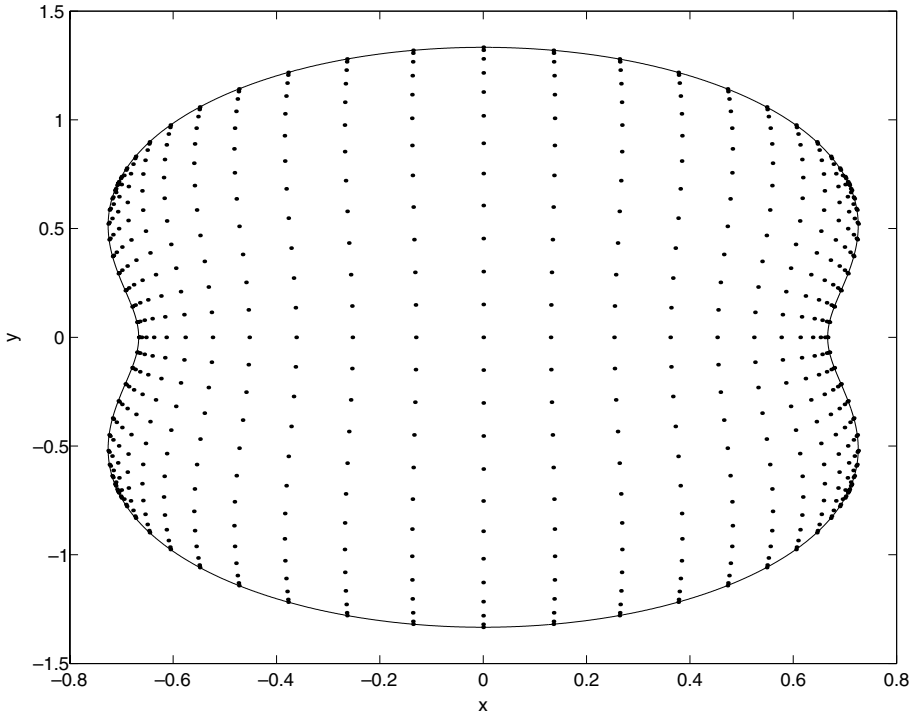

Fig. 3. Collocation nodes on complex geometry ($k = 1$).

the collocation nodes near the four corners are mapped onto nodes outside the domain (see Fig. 5). Hence for increasing oscillations of the boundary the present approach should not be used. But for moderate oscillations of the boundary curve we obtained a high order method. For more complex domains we also tested the polar coordinate approach. The mapping is given by

$$\begin{pmatrix} x \\ y \end{pmatrix} = r \begin{pmatrix} d(\theta)\cos(\theta) \\ d(\theta)\sin(\theta) \end{pmatrix}, \quad 0 \leqslant r \leqslant 1, \;\; 0 \leqslant \theta < 2\pi. \tag{13}$$

We have to transform the Laplace operator into the polar coordinates. For this purpose we introduce the following abbreviations:

$$d = d(\theta), \quad d' = d'(\theta), \quad d'' = d''(\theta), \quad c = \cos(\theta), \quad s = \sin(\theta).$$

The partial derivatives are now transformed as follows:

$$\begin{bmatrix} a_{11} & a_{12} & a_{13} & 0 & 0 \\ a_{21} & a_{22} & a_{23} & 0 & 0 \\ a_{31} & a_{32} & a_{33} & a_{34} & a_{35} \\ 0 & 0 & 0 & a_{44} & a_{45} \\ 0 & 0 & 0 & a_{54} & a_{55} \end{bmatrix} \begin{bmatrix} u_{xx} \\ u_{xy} \\ u_{yy} \\ u_x/r \\ u_y/r \end{bmatrix} = \begin{bmatrix} u_{rr} \\ (ru_{r\theta} - u_\theta)/r^2 \\ u_{\theta\theta}/r^2 \\ u_r/r \\ u_\theta/r^2 \end{bmatrix}, \tag{14}$$

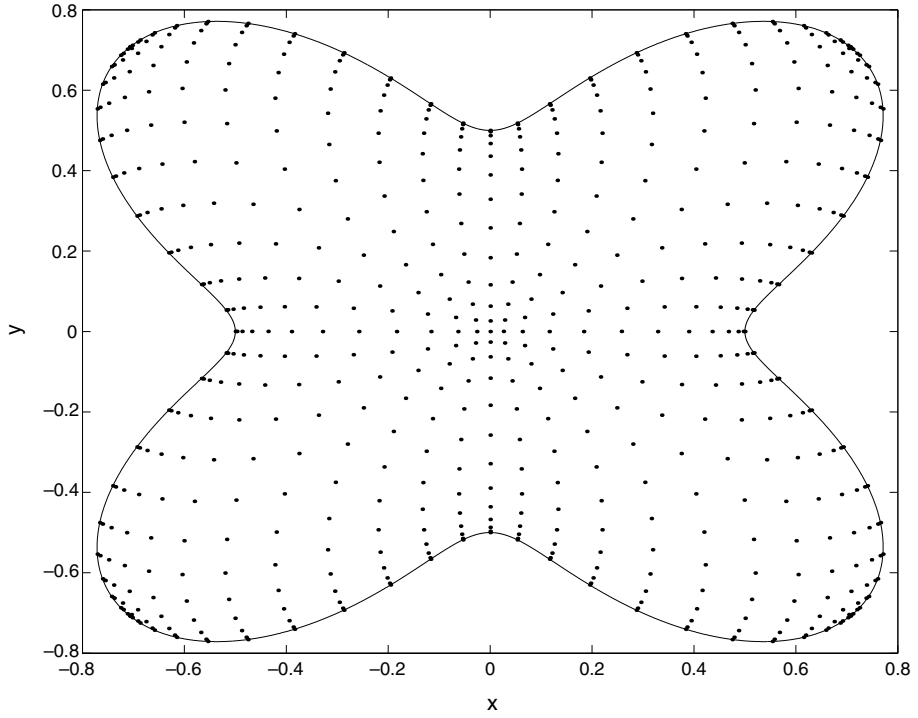

Fig. 4. Collocation nodes on complex geometry ($k = 2$).

Table 4
Numerical results for example (4) with Gordon and Hall

N	$k = 0$		$k = 1$		$k = 2$	
	E_2	E_2^{p}	E_2	E_2^{p}	E_2	E_2^{p}
8	8.73×10^{-2}	1.36×10^{-1}	2.08×10^{-1}	2.08×10^{-1}	3.25×10^{-1}	2.35×10^{-1}
16	7.81×10^{-6}	9.77×10^{-5}	1.25×10^{-3}	3.13×10^{-3}	3.03×10^{-2}	3.89×10^{-3}
24	1.60×10^{-11}	8.23×10^{-9}	5.10×10^{-5}	1.12×10^{-5}	3.59×10^{-3}	3.79×10^{-5}
32	2.10×10^{-13}	2.99×10^{-13}	4.15×10^{-6}	1.68×10^{-8}	5.08×10^{-4}	2.77×10^{-7}
48	8.21×10^{-13}	8.35×10^{-13}	4.16×10^{-8}	8.21×10^{-13}	1.69×10^{-5}	6.63×10^{-12}
64	2.32×10^{-12}	2.20×10^{-12}	5.34×10^{-10}	2.21×10^{-12}	9.33×10^{-7}	2.07×10^{-12}

Table 5
Numerical results for example (5) with Gordon and Hall

N	$k = 0$		$k = 1$		$k = 2$	
	E_2	E_2^{p}	E_2	E_2^{p}	E_2	E_2^{p}
8	8.58×10^{-6}	1.26×10^{-6}	9.30×10^{-4}	1.78×10^{-4}	4.25×10^{-3}	1.93×10^{-3}
16	1.71×10^{-9}	1.14×10^{-12}	3.69×10^{-5}	7.91×10^{-9}	4.66×10^{-4}	3.61×10^{-7}
24	5.47×10^{-13}	4.84×10^{-14}	2.65×10^{-6}	4.51×10^{-13}	5.98×10^{-5}	1.33×10^{-10}
32	8.22×10^{-14}	9.65×10^{-14}	2.33×10^{-7}	7.89×10^{-14}	8.63×10^{-6}	8.73×10^{-14}
48	8.11×10^{-13}	7.65×10^{-13}	2.42×10^{-9}	5.80×10^{-13}	2.96×10^{-7}	1.18×10^{-12}
64	1.50×10^{-12}	1.37×10^{-12}	3.13×10^{-11}	1.17×10^{-12}	1.73×10^{-8}	2.98×10^{-12}

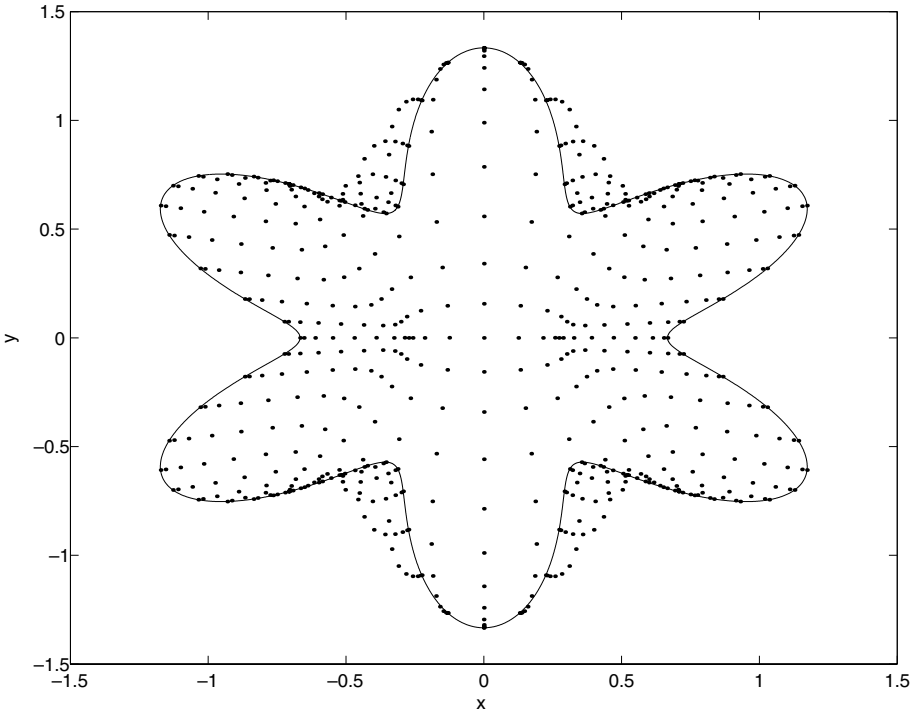

Fig. 5. Collocation nodes on complex geometry ($k = 3$).

where $A = (a_{ij}), i, j = 1, 2, 3$ is given by

$$A = \begin{bmatrix} d^2c^2 & 2csd^2 & d^2s^2 \\ dc(d'c - ds) & d^2(c^2 - s^2) + 2dd'cs & ds(d's + dc) \\ (d'c - ds)^2 & 2(d'^2 - d^2)sc + 2dd'(c^2 - s^2) & (d's + dc)^2 \end{bmatrix}$$

and the other components are

$$a_{34} = d''c - 2d's - dc, \quad a_{35} = d''s + 2d'c - ds,$$

$$a_{44} = dc, \quad a_{45} = ds, \quad a_{54} = d'c - ds, \quad a_{55} = d's + dc.$$

By inverting the above matrix and taking the sum of the first and third row we exactly obtain the coefficients of the transformed Laplace operator in polar coordinates. Now we are able to apply spectral collocation schemes. Here we follow the approach of Chen et al. [4]. In the radius r they employ Chebyshev Gauss–Radau collocation nodes given by

$$r_j = \frac{1}{2}\left(1 + \cos\frac{2\pi j}{2N_r + 1}\right), \quad j = 0, \ldots, N_r.$$

The center $r = 0$ is avoided and hence no extra pole condition is required. The corresponding transformation matrix T now results in

$$T = \left(\cos\frac{2\pi jk}{2N_r + 1}\right), \quad j, k = 0, \ldots, N_r.$$

The derivatives in r can be constructed in the same way as in Section 3. The derivatives in θ are obtained by Fourier collocation [3]. The collocation nodes are equidistant, i.e.,

$$\theta_j = \frac{2\pi j}{N_\theta}, \quad j = 0, \ldots, N_\theta - 1.$$

The derivative matrix is explicitly given by

$$\left(D_{N_\theta}\right)_{kj} = \begin{cases} \frac{1}{2}(-1)^{k+j} \cot\frac{(k-j)\pi}{N_\theta} & k \neq j, \\ 0 & k = j. \end{cases}$$

Partial derivatives are derived by tensor product representation. In our applications we choose

$$N_r = N, \quad N_\theta = 2N.$$

We performed numerical simulations for the examples (4) and (5). The errors in the discrete L^2- and L^∞-norms were calculated. The boundary curve is once more given by (11) with $k = 1, 2, 3$. Here we observe that also for increasing k we obtain reasonable distributions of collocation nodes (see Figs. 6 and 7 for $k = 2, 3$ and $N = 16$). Clearly, due to the high oscillation of the solution we obtain less favorable results for example (4) (see Table 6). Here the mapping of Gordon and Hall yields much better results. The difference between polar coordinates and our mapping technique becomes more striking for example (5) (see Table 7). For $N = 32$ we always obtain machine accuracy with an error of about 10^{-14}. For increasing complexity of the domain ($k \geqslant 3$) we recommend a decomposition of the domain so that on each subdomain the proposed mapping technique can be employed.

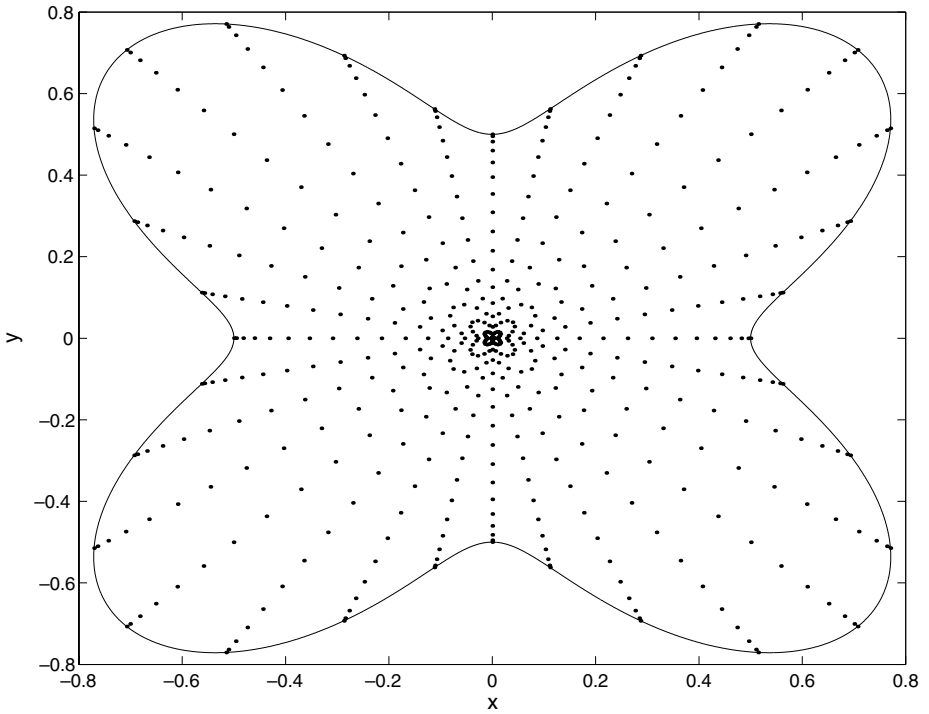

Fig. 6. Collocation nodes with polar coordinates ($k = 2$).

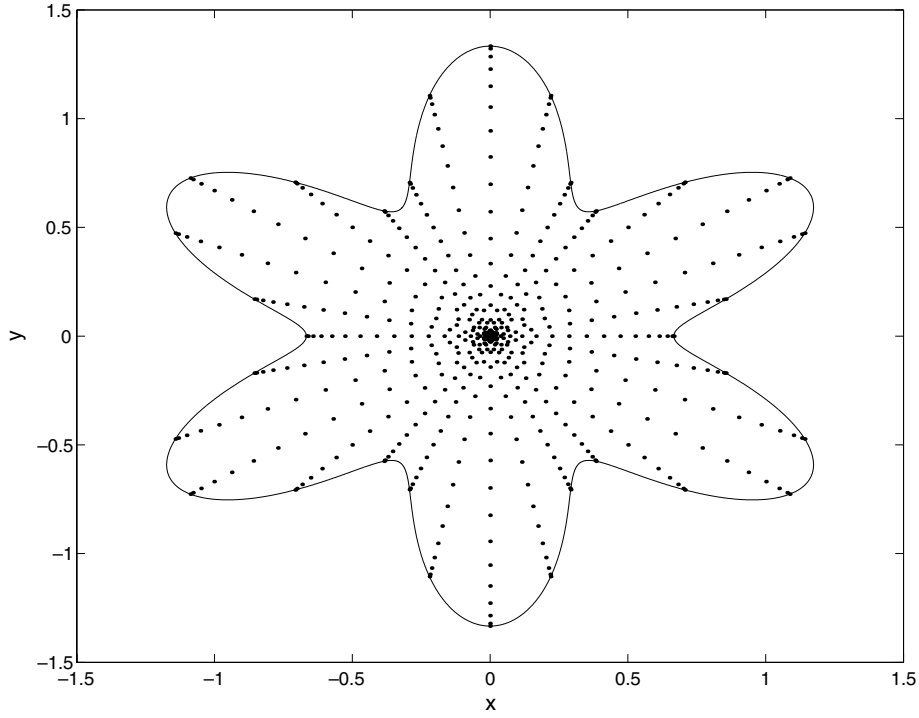

Fig. 7. Collocation nodes with polar coordinates ($k = 3$).

Table 6
Numerical results for example (4) with Chen's polar coordinates

N	$k = 1$		$k = 2$		$k = 3$	
	E_2	E_∞	E_2	E_∞	E_2	E_∞
8	1.91×10^{0}	2.82×10^{0}	2.58×10^{0}	4.99×10^{0}	1.14×10^{0}	2.34×10^{0}
16	5.81×10^{-2}	1.46×10^{-1}	3.09×10^{-1}	5.93×10^{-1}	4.29×10^{-1}	1.43×10^{0}
24	2.58×10^{-3}	3.65×10^{-3}	2.02×10^{-2}	3.79×10^{-2}	1.87×10^{-1}	5.94×10^{-1}
32	1.28×10^{-5}	1.77×10^{-5}	2.11×10^{-3}	2.69×10^{-3}	4.20×10^{-2}	1.24×10^{-1}
48	1.66×10^{-11}	2.41×10^{-11}	1.34×10^{-6}	1.66×10^{-6}	1.03×10^{-3}	3.45×10^{-3}
62	3.21×10^{-12}	1.58×10^{-11}	4.51×10^{-10}	5.42×10^{-10}	1.42×10^{-4}	1.80×10^{-4}

Table 7
Numerical results for example (5) with Chen's polar coordinates

N	$k = 1$		$k = 2$		$k = 3$	
	E_2	E_∞	E_2	E_∞	E_2	E_∞
8	1.10×10^{-2}	1.40×10^{-2}	1.31×10^{-1}	2.31×10^{-1}	1.91×10^{-1}	4.06×10^{-1}
16	2.38×10^{-7}	3.64×10^{-7}	1.07×10^{-3}	1.65×10^{-3}	1.63×10^{-2}	4.15×10^{-2}
24	2.97×10^{-11}	3.39×10^{-11}	2.42×10^{-6}	3.00×10^{-6}	1.22×10^{-3}	2.16×10^{-3}
32	2.48×10^{-12}	8.23×10^{-12}	3.59×10^{-9}	4.15×10^{-9}	1.65×10^{-6}	1.06×10^{-5}
48	4.79×10^{-12}	2.37×10^{-11}	2.10×10^{-12}	9.46×10^{-12}	2.00×10^{-9}	2.70×10^{-9}

6. Improved polar coordinate approach

Here we introduce polar coordinates (r,θ) and the transformed equation on the unit disc D reads as follows:

$$r^2 u_{rr} + r u_r + u_{\theta\theta} = r^2 f. \tag{15}$$

For stability reasons the original equation was multiplied by r^2. Usually one considers $r \in [0,1]$ and $\theta \in [0,2\pi]$ and one employs Chebyshev collocation in r and Fourier collocation in θ. Here we allow $r \in [-1,1]$ and $\theta \in [0,2\pi]$. In r we employ the standard Chebyshev Gauss–Lobatto nodes given by

$$r_i = \cos\frac{i\pi}{N_r}, \quad i = 0,\ldots,N_r.$$

In order to avoid an overlap of collocation nodes the discrete angles θ_j are given by

$$\theta_j = \begin{cases} j\frac{\pi}{N} & j = 0,\ldots,N-1, \\ \pi + \frac{\pi}{2N} + (j-N)\frac{\pi}{N} & j = N,\ldots,2N-1. \end{cases} \tag{16}$$

For given N (N even) we choose

$$N_r = N-1, \quad N_\theta = 2N.$$

Since $N_r = N-1$ is odd the center $r = 0$ is not a collocation point. By this choice we avoid some extra pole condition. In Figs. 8 and 9 we plotted the collocation nodes of Chen et al. and our method for $N = 16$. Clearly, the nodes of Chen are clustering near the center whereas our nodes keep far away from $r = 0$. In the numerical simulations this leads to an improved condition number. Let us first describe the spectral collocation scheme in r. First one has to introduce the transformation matrices from physical space to coefficient space. Since we employ a Chebyshev expansion we obtain the following matrix:

$$T = \cos\left(k\frac{i\pi}{N_r}\right), \quad i,k = 0,\ldots,N_r.$$

Further we need the differentiation matrix in the Chebyshev coefficient space which is explicitly given by $\hat{D} = (d_{i,j}) \in \mathbb{R}^{N_r+1,N_r+1}$. Now we are once more able to write the spectral derivative matrices D1 and D2 for the first and second derivatives. They are explicitly given by

$$\mathrm{D1} = T\hat{D}T^{-1}, \quad \mathrm{D2} = T\hat{D}^2T^{-1}.$$

The spectral operators can be efficiently evaluated by fast Fourier transforms (FFTs) in $O(N_r \log N_r)$ arithmetic operations. The derivatives in θ are derived in a similar fashion. First we introduce the (real) Fourier basis

$$\phi_k(x) = \begin{cases} \sin(k+1)x & k = 0,\ldots,N-2, \\ \cos Nx + \sin Nx & k = N-1, \\ \cos(k-N)x & k = N,\ldots,2N-1. \end{cases}$$

The corresponding transformation matrix in Fourier space is now defined as follows:

$$T_\theta = \big(\phi_k(\theta_j)\big), \quad j,k = 0,\ldots,2N-1,$$

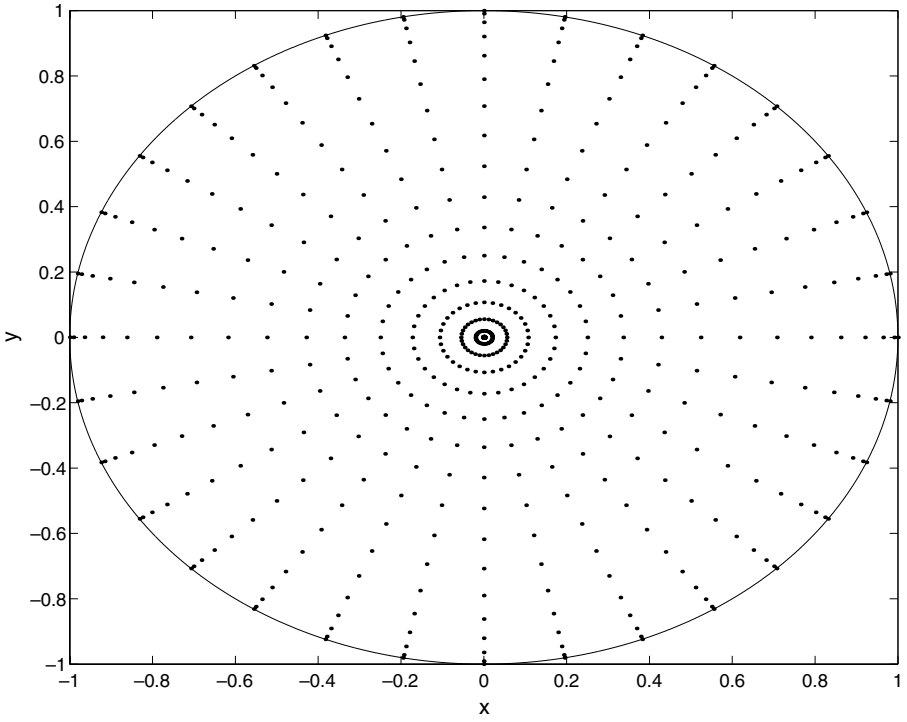

Fig. 8. Collocation nodes of Chen et al.

where the nodes θ_j are given in (4). The second derivative in coefficient space is

$$\hat{D}_\theta^2 = \begin{cases} -\mathrm{diag}((k+1)^2) & k = 0, \ldots, N-1, \\ -\mathrm{diag}((k-N)^2) & k = N, \ldots, 2N-1. \end{cases}$$

Now the second derivative in Fourier space reads as

$$\mathrm{D2}_\theta = T_\theta \hat{D}_\theta^2 T_\theta^{-1}.$$

The first derivative can be constructed as follows. We first evaluate

$$\phi_k'(\theta_j) = \begin{cases} (k+1)\cos(k+1)\theta_j & k = 0, \ldots, N-2, \;\; j = 0, \ldots, 2N-1, \\ N\cos j\pi & k = N-1, \;\; j = 0, \ldots, N-1, \\ -N\cos j\pi & k = N-1, \;\; j = N, \ldots, 2N-1, \\ -(k-N)\sin(k-N)\theta_j & k = N, \ldots, 2N-1, \;\; j = 0, \ldots, 2N-1 \end{cases}$$

and then obtain with $D_\theta = (\phi_k'(\theta_j))$

$$\mathrm{D1}_\theta = D_\theta T_\theta^{-1}.$$

By tensor product representation it is once more an easy task to write the spectral partial derivatives in 2D. First we compared the condition numbers of our approach and the approach of Chen et al. [4]. They are numerically evaluated in the spectral norm. From the numerical results in Table 8 we observe that the

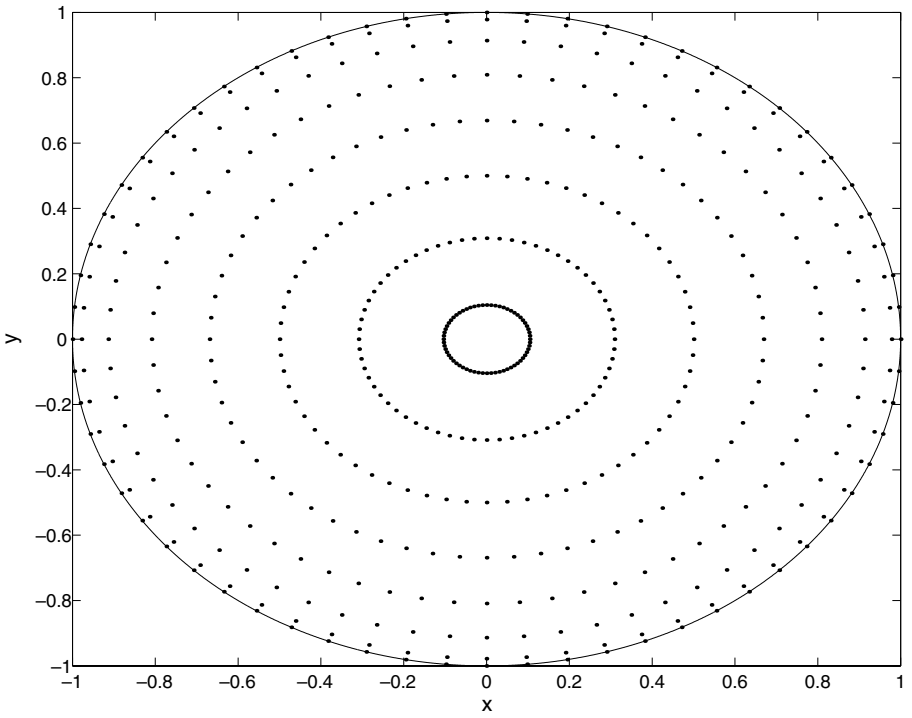

Fig. 9. Collocation nodes with our method.

Table 8
Condition numbers

N	Present method	Chen et al.
8	3.79×10^2	1.82×10^4
16	1.08×10^4	3.70×10^5
24	7.37×10^4	2.17×10^6
32	2.82×10^5	7.62×10^7
48	1.81×10^6	4.45×10^7
62	5.76×10^6	1.35×10^8

condition number of the spectral operator introduced by Chen is about 2–3 digits larger than for the present method. Hence for time-dependent problems our approach leads to less restrictive time limitations. However, we consider stationary problems and are interested in the global accuracy of the method. For this purpose we calculated the discrete L^2-errors $\|u - u_N\|_2$. We once more consider the two examples (4) and (5) introduced in [4,5,16]. From the Tables 9 and 10 we observe the high spectral accuracy for both methods. Due to the large condition number of Chen's method the accuracy is somewhat disturbed for increasing N. For example (5) with $N = 32$ there is a loss of 3 digits in accuracy compared to our method. The numerical results substantiate the usefulness of our new approach.

Once more we consider the Poisson problem on domains with smooth boundaries Γ which are parameterized in the arc length θ. The mapping is given by

$$\begin{pmatrix} x \\ y \end{pmatrix} = (d(\theta)r + b(\theta)) \begin{pmatrix} \cos(\theta) \\ \sin(\theta) \end{pmatrix}, \quad -1 \leqslant r \leqslant 1, \;\; 0 \leqslant \theta < 2\pi, \tag{17}$$

Table 9
Numerical results for example (4)

N	Present method	Chen et al.
8	1.73×10^{0}	2.33×10^{0}
16	3.67×10^{-3}	3.42×10^{-3}
24	1.03×10^{-7}	6.00×10^{-9}
32	2.04×10^{-13}	1.75×10^{-11}

Table 10
Numerical results for example (5)

N	Present method	Chen et al.
8	2.28×10^{-6}	2.86×10^{-6}
16	1.03×10^{-14}	1.78×10^{-13}
24	6.62×10^{-14}	2.47×10^{-11}
32	7.02×10^{-14}	2.34×10^{-11}

where

$$d(\theta) = \frac{r_2(\theta) - r_1(\theta)}{2}, \quad b(\theta) = \frac{r_2(\theta) + r_1(\theta)}{2}.$$

Here r_1, r_2 denote the distances of the boundary curve from the center $r = 0$. We have to transform the Laplace operator into the polar coordinates. For this purpose we introduce the following abbreviations:

$$d = d(\theta), \quad c = \cos(\theta), \quad s = \sin(\theta).$$

The partial derivatives are now transformed as follows:

$$\begin{bmatrix} (dc)^2 & 2csd^2 & (ds)^2 & 0 & 0 \\ dcx_\theta & dsx_\theta + dcy_\theta & dsy_\theta & (dc)_\theta & (ds)_\theta \\ x_\theta^2 & 2x_\theta y_\theta & y_\theta^2 & x_{\theta\theta} & y_{\theta\theta} \\ 0 & 0 & 0 & dc & ds \\ 0 & 0 & 0 & x_\theta & y_\theta \end{bmatrix} \begin{bmatrix} u_{xx} \\ u_{xy} \\ u_{yy} \\ u_x \\ u_y \end{bmatrix} = \begin{bmatrix} u_{rr} \\ u_{r\theta} \\ u_{\theta\theta} \\ u_r \\ u_\theta \end{bmatrix}. \tag{18}$$

By inverting the above matrix and taking the sum of the first and third row we exactly obtain the coefficients of the transformed Laplace operator in polar coordinates. Now we are able to apply spectral collocation schemes in the same manner as before. We consider boundary curves with $b \equiv 0$ and d given by (11) and (12). For $k = 0$ we reobtain the unit disc and for $k = 1, 2, 3$ increasing mode numbers of the boundary curve are considered. In the Figs. 10–12 we plotted the distribution of collocation nodes for $k = 1, 2, 3$ and $N = 16$. We performed numerical simulations for the examples (4) and (5). The errors E_2, E_∞ in the discrete L^2- and L^∞-norms were calculated. For example (5), $k = 1$ we obtain for $N = 32$ the machine accuracy with an error of about 10^{-14} (see Table 12). Clearly, due to the high oscillation of the solution we obtain less favorable results for example (4) (see Table 11). For increasing complexity of the problem (solution or domain) we recommend a decomposition of the domain so that on each subdomain the proposed mapping technique can be employed.

Finally we compared our approach with the existing literature on diameter expansions. Also Fornberg [6,7] recommends the expansion over diameters as a means of avoiding the serious clustering at the origin.

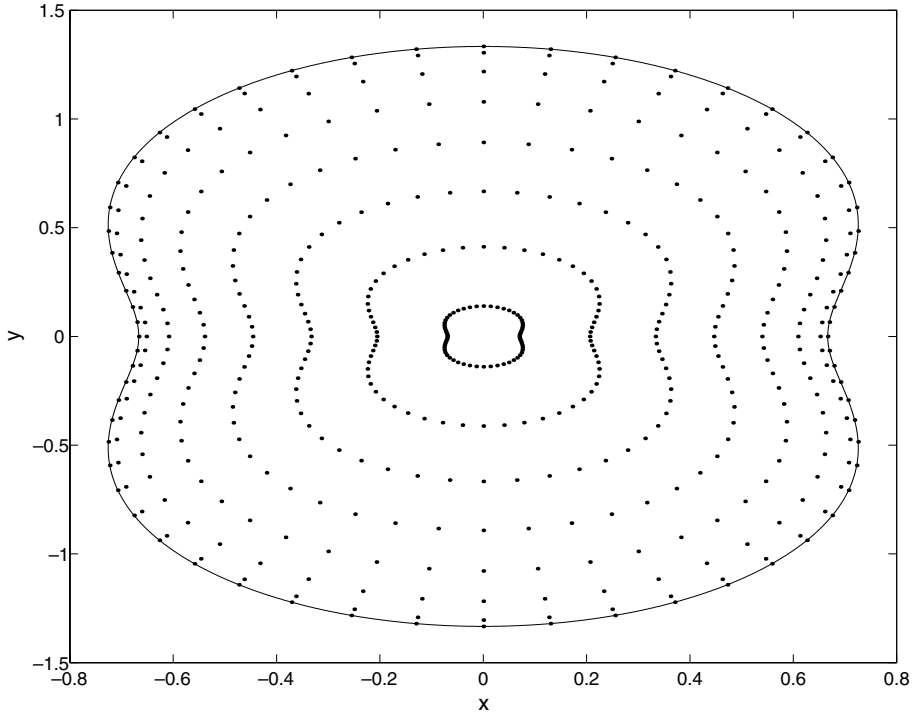

Fig. 10. Collocation nodes on complex geometry ($k = 1$).

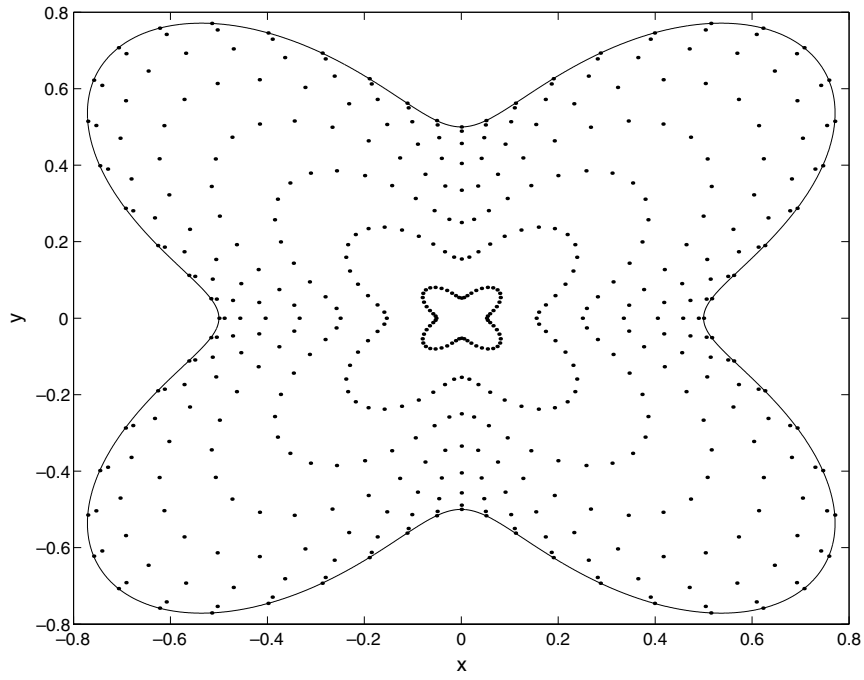

Fig. 11. Collocation nodes on complex geometry ($k = 2$).

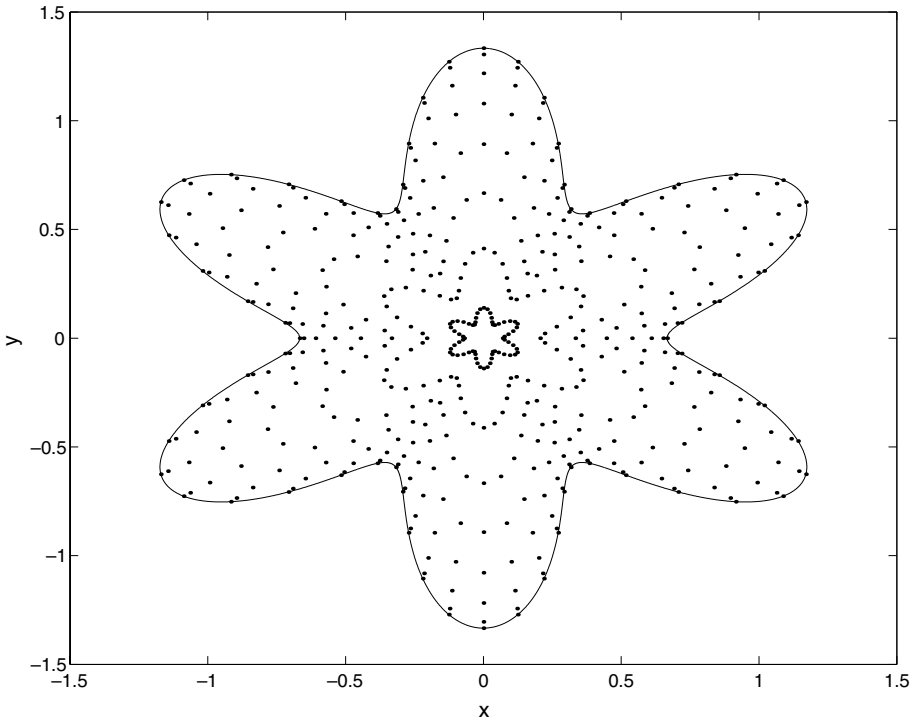

Fig. 12. Collocation nodes on complex geometry ($k = 3$).

Table 11
Numerical results for example (4) with the diameter approach

N	$k = 1$		$k = 2$		$k = 3$	
	E_2	E_∞	E_2	E_∞	E_2	E_∞
8	1.40×10^{0}	3.57×10^{0}	7.62×10^{-1}	2.70×10^{0}	1.92×10^{0}	6.31×10^{0}
16	1.53×10^{-1}	9.28×10^{-1}	2.39×10^{-1}	1.43×10^{0}	1.09×10^{0}	5.43×10^{0}
24	3.04×10^{-3}	2.15×10^{-2}	1.34×10^{-2}	1.12×10^{-1}	4.13×10^{-1}	3.32×10^{0}
32	1.52×10^{-5}	1.28×10^{-4}	7.39×10^{-4}	7.13×10^{-3}	1.05×10^{-1}	1.10×10^{0}
48	2.65×10^{-11}	3.02×10^{-10}	1.53×10^{-7}	2.31×10^{-6}	5.09×10^{-3}	4.29×10^{-2}
62	3.42×10^{-13}	1.00×10^{-12}	3.70×10^{-10}	3.28×10^{-9}	1.71×10^{-4}	1.60×10^{-3}

Table 12
Numerical results for example (5) with the diameter approach

N	$k = 1$		$k = 2$		$k = 3$	
	E_2	E_∞	E_2	E_∞	E_2	E_∞
8	4.18×10^{-3}	1.63×10^{-2}	4.86×10^{-2}	1.46×10^{-1}	5.57×10^{-1}	2.55×10^{0}
16	5.48×10^{-7}	2.92×10^{-6}	6.68×10^{-4}	2.69×10^{-3}	3.85×10^{-2}	1.77×10^{-1}
24	1.82×10^{-11}	9.84×10^{-11}	1.19×10^{-6}	6.17×10^{-6}	5.91×10^{-4}	3.39×10^{-3}
32	6.70×10^{-14}	2.20×10^{-13}	1.60×10^{-9}	9.52×10^{-9}	5.13×10^{-5}	3.89×10^{-4}
48	9.74×10^{-14}	3.86×10^{-13}	1.01×10^{-13}	3.63×10^{-13}	7.67×10^{-9}	6.91×10^{-8}

An efficient implementation was presented by Shen [22] and in MATLAB by Trefethen [24]. Fornberg first writes the complete collocation system where grid values at symmetric points occur twice. This is due to the fact that the mapping form (r,θ) to (x,y) is 2-to-1. Then the redundant equations are eliminated by using the symmetry condition

$$u(r,\theta) = u(-r,\theta+\pi).$$

We do not need such an elimination process since we avoid a double gridding by shifting the θ-grid for $\theta > \pi$. If the same collocation grids are used then Fornbergs and our approach should yield the same spectral approximation. But in fact, Fornberg uses the double amount of collocation nodes in r, i.e., $N_r = 2N-1$ and only the half amount of nodes in θ, i.e., $N_\theta = N$. We think that our grid is more appropriate for the diameter approach since the numbers of collocation conditions are chosen in accordance to the polynomial degrees in r and θ. Due to the substantial regularity of the solution it is not reasonable to use about $2N$ conditions of collocation for a polynomial of degree N in r. On the other hand, we allow a better resolution in θ with twice the amount of collocation nodes. We think that Fornbergs grid is well suited for the radius approach but not for the diameter approach. Torres and Coutsias [23] use the diameter approach for the spectral tau scheme with parity-adjusted basis functions. By converting the Chebyshev operator into an equivalent (well conditioned) tridiagonal form, no additional pole condition or other regularization is required for the Poisson problem. On the other hand, the Helmholtz operator poses serious conditioning problems. A direct compare to our collocation scheme is not possible since the tau method with parity-adjusted basis functions yields a very different approach. Huang et al. [17] show that imposition of one pole condition (i.e. vanishing at $r = 0$ to some fixed, low order only regardless of Fourier mode number) suffices for regularity of solutions of the Poisson problem. A further discussion of pole conditions can also be found in Boyd [2]. We do not claim the superiority of the odd grid for the diameter approach. With suitable pole conditions and/or proper care for parity the choice of even or odd grids makes little difference.

7. Conclusion

Poisson problems on the unit disc are solved by spectral collocation schemes based on the mapping of Gordon and Hall. The problems of polar coordinate approaches with a singularity in $r = 0$ are avoided and the well known high spectral accuracy is maintained. For a comparison we present numerical results which show the good performance of our new approach. Furthermore we present a diameter approach where the collocation nodes are not clustering near the center. Hence the condition number of the spectral operator is improved. Finally it is also shown that the methods can be successfully applied to more complex domains.

References

[1] C. Bernardi, A. Karageorghis, Spectral method in a part of a disc, Numer. Math. 73 (1996) 265–289.
[2] J.P. Boyd, Chebyshev & Fourier Spectral Methods, second ed., Dover, New York, 2001.
[3] C. Canuto, M.Y. Hussaini, A. Quarteroni, T.A. Zang, Spectral Methods in Fluid Dynamics, Springer Series in Computational Physics, Springer-Verlag, Berlin, 1989.
[4] H. Chen, Y.S. Su, D. Shizgal, A direct spectral collocation Poisson solver in polar and cylindrical coordinates, J. Comp. Phys. 160 (2000) 453–463.
[5] H. Eisen, W. Heinrichs, K. Witsch, Spectral methods and polar coordinate singularities, J. Comp. Phys. 96 (1991) 241–257.
[6] B. Fornberg, D.M. Sloan, A review of pseudospectral methods for solving partial differential equations, Acta Numerica 1994 (1994) 203–267.
[7] B. Fornberg, A pseudospectral approach for polar and spherical geometries, SIAM J. Sci. Comput. 16 (1995) 1071–1081.
[8] W.J. Gordon, C.A. Hall, Construction of curvilinear co-ordinate systems and their applications to mesh generation, Int. J. Numer. Meth. Eng. 7 (1973) 461–477.

[9] W.J. Gordon, C.A. Hall, Transfinite element methods: blending-function interpolation over arbitrary curved element domains, Numer. Math. 21 (1973) 109–129.
[10] D. Gottlieb, S.A. Orszag, Numerical Analysis of spectral methods: theory and applications. CBMS-NSF Regional Conference Series in Applied Mathematics No. 26, SIAM, Philadelphia, 1977.
[11] H. Haschke, W. Heinrichs, Splitting techniques with staggered grids for the Navier–Stokes equations in the 2D case, J. Comp. Phys. 168 (2001) 131–154.
[12] W. Heinrichs, Splitting techniques for the pseudospectral approximation of the unsteady Stokes equations, SIAM J. Numer. Anal. 30 (1993) 19–39.
[13] W. Heinrichs, Splitting techniques for the unsteady Stokes equations, SIAM J. Numer. Anal. 35 (1998) 1646–1662.
[14] W. Heinrichs, Spectral collocation on triangular elements, J. Comp. Phys. 145 (1998) 743–757.
[15] W. Heinrichs, B. Loch, Spectral schemes on triangular elements, J. Comp. Phys. 173 (2001) 279–301.
[16] W. Huang, D.M. Sloan, Pole condition for singular problems, J. Comp. Phys. 107 (1993) 254–261.
[17] W. Huang, H. Ma, W. Sun, Convergence analysis of pseudospectral methods for solving partial differential equations in polar and cylindrical geometries, Preprint 2002.
[18] A. Karageorghis, Conforming spectral methods for Poisson problems in cuboidal domains, J. Sci. Comput. 9 (1994) 341–349.
[19] T. Matsushima, P.S. Marcus, A spectral method for polar coordinates, J. Comp. Phys. 120 (1995) 365–374.
[20] S.A. Orszag, Spectral methods for problems in complex geometries, J. Comp. Phys. 37 (1980) 70–92.
[21] J. Shen, Efficient spectral–Galerkin methods III: polar and cylindrical geometries, SIAM J. Sci. Comput. 18 (1997) 1583–1604.
[22] J. Shen, A new fast Chebyshev–Fourier algorithm for Poisson-type equations in polar geometries, Appl. Numer. Math. 33 (2000) 183–190.
[23] D.J. Torres, E.A. Coutsias, Pseudospectral solution of the 2D Navier–Stokes equations in a disc, SIAM J. Sci. Comput. 21 (1999) 378–403.
[24] L.N. Trefethen, Spectral Methods in Matlab, SIAM, Philadelphia, 2000.